

# Onset of ring defects in n-type Czochralski-grown silicon wafers

Cite as: J. Appl. Phys. 127, 153101 (2020); doi: 10.1063/5.0005899

Submitted: 25 February 2020 · Accepted: 27 March 2020 ·

Published Online: 15 April 2020



View Online



Export Citation



CrossMark

Rabin Basnet,<sup>1,a)</sup> Sieu Pheng Phang,<sup>1</sup> Chang Sun,<sup>1</sup> Fiacre E. Rougier,<sup>2</sup> and Daniel Macdonald<sup>1</sup>

## AFFILIATIONS

<sup>1</sup> Research School of Electrical, Energy and Materials Engineering, The Australian National University, Canberra, ACT 2601, Australia

<sup>2</sup> School of Photovoltaic and Renewable Energy Engineering, The University of New South Wales, Sydney, New South Wales 2052, Australia

<sup>a)</sup>Author to whom correspondence should be addressed: rabin.basnet@anu.edu.au

## ABSTRACT

This paper presents experimental studies on the formation of ring defects during high-temperature annealing in both electronic-grade and upgraded metallurgical-grade (UMG) Czochralski-grown silicon wafers. Generally, a faster onset of ring defects, or shorter incubation time, was observed in the UMG samples ( $[O_i] = 6.3 \times 10^{17} \text{ cm}^{-3}$ ) in comparison to the electronic-grade samples ( $[O_i] = 3.9 \times 10^{17} \text{ cm}^{-3}$ ) used in this work. By applying a *tabula rasa* (TR) treatment prior to annealing, the incubation time can be increased for both types of wafers. We show that TR temperatures above 1000 °C are necessary to effectively dissolve grown-in oxygen precipitate nuclei and limit the subsequent formation of ring defects. A 30 min TR treatment at 1000 °C resulted in the longest incubation time for both types of samples used in this work, as it achieved the best balance between precipitate nuclei dissolution and precipitate re-growth/ripening. Finally, a nitrogen ambient TR step showed a short incubation time for the formation of ring defects in comparison to an oxygen ambient TR step.

Published under license by AIP Publishing. <https://doi.org/10.1063/5.0005899>

## I. INTRODUCTION

Czochralski-grown silicon (Cz-Si) wafers are emerging as the most commonly used wafers for solar cell fabrication. Cz-Si typically contains  $10^{17}$  to  $10^{18} \text{ cm}^{-3}$  of oxygen impurities, which occur in the form of interstitials, thermal donors, or precipitates. Depending on the ingot growth conditions, parts of the ingot can be either vacancy- or interstitial-rich, or mixed. This intrinsic point-defect concentration influences oxygen precipitation<sup>1</sup> and may contribute to the formation of oxidation-induced stacking faults (OSFs).<sup>2</sup> In general, both thermal donors and oxygen precipitate-induced defects can appear as ring-like defects in photoluminescence (PL) images of Cz-Si wafers.<sup>3,4</sup> Fortunately, thermal donors are annihilated at temperatures above 650 °C, meaning they have no impact on homo-junction solar cells.<sup>5,6</sup> However, grown-in oxygen precipitate nuclei (OPN) can grow during high-temperature steps during solar cell fabrication,<sup>7</sup> resulting in increased recombination activity.<sup>3,8–10</sup> In some cases, Cz-Si wafers develop ring defects owing to the strong recombination activity of oxygen precipitates and their associated extended defects.<sup>11,12</sup> Ring defects influence the uniformity of the electrical properties of the wafer and can contribute up to 4% (absolute) loss in solar cell efficiency.<sup>3</sup>

Thus, it is crucial to understand the formation of ring defects and to devise methods to mitigate their negative impact on the performance of solar cells.

Numerous works have demonstrated different methods to mitigate the impact of oxygen precipitates and ring defects in silicon solar cells. One such method is phosphorus diffusion gettering (PDG), which can reduce the recombination activity of oxygen precipitates and ring defects<sup>13</sup> by removing decorating metallic impurities. Furthermore, hydrogenation can partially passivate oxygen precipitates and ring defects.<sup>14,15</sup> Both of these methods are used as curative steps during solar cell fabrication to mitigate or eliminate the impact of oxygen precipitates. In addition, a pre-fabrication anneal step, known as a *tabula rasa* (TR), can be used as a preventive method to avoid the formation of oxygen precipitates during high-temperature treatments.<sup>12,16–19</sup> Such a process clears the thermal history of the wafers by homogenizing the grown-in defect concentration and dissolving precipitate nuclei, leading to a delayed onset of oxygen precipitation during subsequent high-temperature processing.<sup>20,21</sup> Unfortunately, the TR step is a very high-temperature process during solar cell fabrication, which increases the processing cost as well as introducing a significant risk of contamination.

Therefore, it is critical to optimize the TR conditions for a given solar cell fabrication sequence. This work aims to clarify the extent to which a TR process can delay the onset of oxygen precipitation in both electronic-grade and upgraded metallurgical-grade (UMG) Cz wafers for a range of TR process conditions.

## II. EXPERIMENTAL DETAILS

Two different types of n-type Cz wafers were used in this work. The first were n-type solar-grade wafers grown using UMG silicon feedstock in the framework of the PHOTOSIL project and supplied by Apollon Solar (ingot number ISO10).<sup>22</sup> The second were commercially available electronic-grade (EG) wafers, selected to represent typical Cz wafers used in solar cell manufacture. The densities of phosphorus [P], boron [B], and carbon concentration [C] within the compensated UMG-Cz wafers were measured by secondary ion mass spectrometry (SIMS). The phosphorus concentration in the EG-Cz wafers was determined via dark conductance measurements. The interstitial oxygen concentrations  $[O_i]$  in both types of wafer were measured by Fourier-transform infrared spectroscopy (FTIR) using a Bruker Vertex 80 tool and calibrated using SEMI MF standard 1188-1107. The [C] in the EG-Cz wafers was below the detection limit ( $1.0 \times 10^{16} \text{ cm}^{-3}$ ) of the FTIR at room temperature. The resulting dopant concentrations, [C], and  $[O_i]$ , are summarized in Table I.

All wafers were saw-damage-etched in the tetramethylammonium hydroxide (TMAH) solution to remove 10–12  $\mu\text{m}$  from each side, with final thicknesses of 150  $\mu\text{m}$  and 290  $\mu\text{m}$  for the UMG-Cz and EG-Cz wafers, respectively. Samples were cleaned using standard RCA (Radio Corporation of America) cleaning steps prior to each high-temperature step. To evaluate the impact of the TR step, the sister wafers were divided into three sets, as shown in Fig. 1. Set 1 consists of samples with no TR step, referred to as the as-grown samples. The samples in set 2 went through TR steps in oxygen at various temperatures and are referred to as the TR-O<sub>2</sub> samples. The samples in set 3 went through the TR step in nitrogen at 1100 °C for 30 min and are referred to as the TR-N<sub>2</sub> samples. To further assess the impact of the TR conditions, temperatures, durations, and ambient gases were varied, as shown in Fig. 1. Then, all three sets of samples were subjected to oxidation at 900 °C to drive oxygen precipitation and promote the formation of ring defects. UMG wafers were annealed at 30 min intervals, whereas EG-Cz samples were annealed at 60 min intervals to observe the evolution of ring defects. During all thermal treatments, loading and unloading of the samples was performed at 700 °C with ramp rates of 15 °C/min.

**TABLE I.** Properties of the n-type wafers used in this work.

Parameters	UMG-Cz	EG-Cz
[B] ( $\text{cm}^{-3}$ )	$1.3 \times 10^{16}$	...
[P] ( $\text{cm}^{-3}$ )	$1.7 \times 10^{16}$	$4.5 \times 10^{14}$
Net doping, $n_0$ ( $\text{cm}^{-3}$ )	$4.0 \times 10^{15}$	$4.5 \times 10^{14}$
$[O_i]$ ( $\text{cm}^{-3}$ )	$6.3 \times 10^{17}$	$3.9 \times 10^{17}$
[C] ( $\text{cm}^{-3}$ )	$1.0 \times 10^{16}$	...

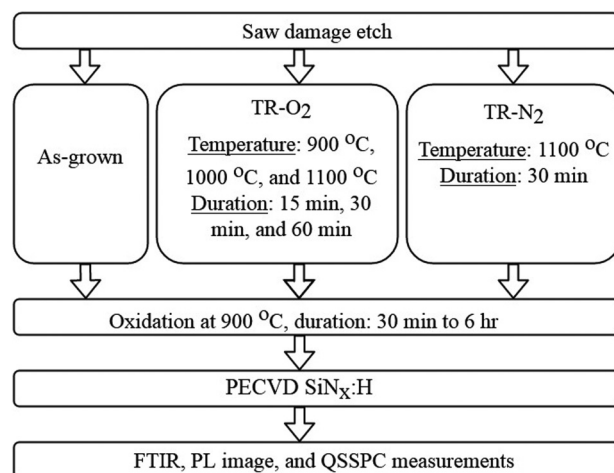


**FIG. 1.** Flow chart of the experimental processes used in this work. Samples were divided into three sets: as-grown, TR-O<sub>2</sub>, and TR-N<sub>2</sub> samples. The SiN<sub>x</sub>:H and oxide layers were removed before FTIR measurements.

Thermal oxide layers formed during the annealing steps were removed by hydrofluoric acid (HF). The  $[O_i]$  in the samples was measured using the infrared absorption band at 1107  $\text{cm}^{-1}$  at room temperature. In this study, radial distributions of  $[O_i]$  were measured by line scans across the samples using a Bruker Hyperion FTIR microscope. The FTIR line scans were conducted using a laser spot size of 10  $\mu\text{m}$  and a spectral resolution of 2  $\text{cm}^{-1}$ . Uncertainty in the  $[O_i]$  measurements arises primarily from variations in wafer thickness, surface roughness, and overlapping of the interstitial oxygen peak and the oxygen precipitate band. The uncertainty in the  $[O_i]$  measurement is estimated to be approximately 10%.

For carrier lifetime measurements and PL images, the samples were passivated using plasma-enhanced chemical vapor deposited (PECVD) silicon nitride (SiN<sub>x</sub>:H) films. SiN<sub>x</sub>:H films were deposited at a substrate temperature of 300 °C for 3 min. This relatively low thermal budget is safely assumed to have no impact on the formation and dissolution of oxygen precipitates. However, the reported lifetimes could be influenced due to hydrogen diffusion during SiN<sub>x</sub>:H films deposition.<sup>23,24</sup> Carrier lifetimes were measured using the quasi-steady state photoconductance and transient photoconductance decay techniques with a WCT-120 tool from Sinton Instruments.<sup>25</sup> The carrier lifetimes of the UMG-Cz wafers were corrected using carrier mobility values for compensated silicon from Schindler's mobility model.<sup>26</sup> PL images were captured using an LIS-R1 PL imaging tool from BT imaging.<sup>27</sup>

## III. RESULTS AND DISCUSSION

### A. Dissolution of grown-in OPN

As expected, after the TR-O<sub>2</sub> steps, we observed an increase in  $[O_i]$  in both types of samples due to the dissolution of grown-in OPN, as shown in Fig. 2. The competing dissolution/growth

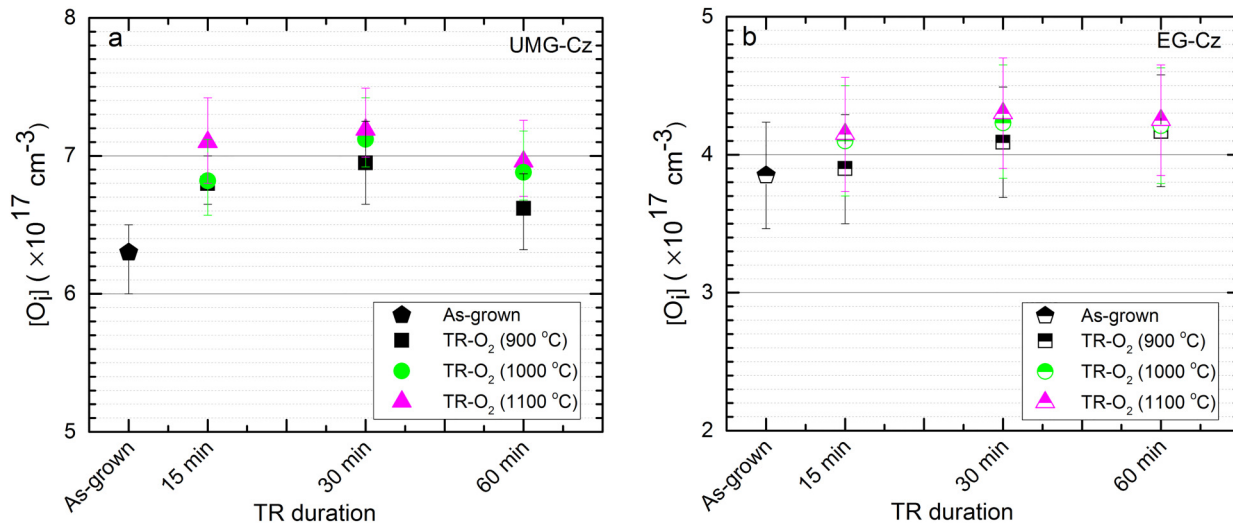


FIG. 2.  $[O_i]$  measured by FTIR in the (a) UMG-Cz and (b) EG-Cz samples after the different TR-O<sub>2</sub> conditions.

behavior of the OPN is governed by a critical radius ( $r_c$ ), which in turn is a function of temperature.<sup>28</sup> If the radius of the grown-in OPN is smaller than  $r_c$ , they shrink and eventually dissolve during annealing. By contrast, the OPN grow if their radius is higher than  $r_c$ . As a result, the increase in  $[O_i]$  was highest at 1100 °C for all the TR durations. Furthermore, during the 30 min TR-O<sub>2</sub> condition, we observed the highest increase in  $[O_i]$  for both types of samples. However, we observed a slightly lower increase in  $[O_i]$  in the 15 min and 60 min TR-O<sub>2</sub> conditions, which could be due to incomplete dissolution of the grown-in OPN and partial regrowth of the undissolved OPN, respectively.<sup>29,30</sup> Moreover, the regrowth rate of undissolved OPN may accelerate in the presence of foreign impurities (e.g., C), reducing  $[O_i]$  more rapidly for the longer anneals in the UMG-Cz wafers.<sup>31,32</sup>

### B. Ring defects in the UMG Cz wafers with different TR durations

Figures 3–5 demonstrate the evolution of ring defects in the as-grown and TR-O<sub>2</sub> UMG-Cz samples during subsequent oxidation at 900 °C, after TR steps of 30, 60, and 15 min duration, respectively. Note that the samples are quartered sections, with the center of the ingot located at the bottom left corner and the edge of the ingot at the top right corner. The effective lifetimes improved after the TR-O<sub>2</sub> steps, suggesting the grown-in OPN were partly limiting the bulk lifetimes in these UMG-Cz samples. However, after subsequent oxidation at 900 °C, the lifetimes degraded and ring defects ultimately appeared in both the as-grown and TR-O<sub>2</sub> UMG-Cz samples. The subsequent degradation was due to increased recombination activity of oxygen precipitates either due to their growth and/or decoration by metallic impurities or extended defects.<sup>33</sup> Therefore, we conclude that TR steps can only delay the formation of ring defects in Cz wafers, rather than

entirely eliminate them. This delay duration, which we refer to as the incubation time, is the specific duration of heat treatment, after which ring defects first appear. For example, the TR-O<sub>2</sub> UMG samples treated at 1100 °C for 30 min showed ring defects after 2 h of subsequent oxidation at 900 °C. Similarly, the TR-O<sub>2</sub> UMG-Cz wafers treated at 1100 °C for 15 min and 60 min had incubation times of 1.5 h and 2 h, respectively, as shown in Figs. 4 and 5. Based on these incubation times, the thermal budget of the solar cell fabrication process can be modified to preserve the bulk lifetime, as shown previously in Ref. 16.

Furthermore, in these UMG-Cz samples, we observed a gradual radial appearance of ring defects. For the as-grown samples, the ring defects first appeared near the center of the ingot (bottom left of the images) after 1.5 h of annealing at 900 °C, as shown in Fig. 3. The rings then expanded toward the edge of the ingot after further oxidation, before finally forming a solid disk. This could be due to the pre-existing vacancy gradient in the as-grown samples, where the vacancy concentration is higher at the center region of the ingot due to the temperature gradient induced by relatively fast-pulling rates of the ingot.<sup>1,34</sup> Furthermore, this growth condition might cause the presence of non-uniform sized grown-in OPN during ingot cooling. Therefore, during the subsequent oxidation, the center part of the samples lost more  $[O_i]$ , as confirmed by the FTIR scans of  $[O_i]$ , as shown in Fig. 6(a).

By contrast, in some of the TR-O<sub>2</sub> samples, the first hint of rings appeared near the edge of the samples, as opposed to the center (e.g., after 2 h of oxidation at 900 °C for 1000 °C and 1100 °C TR-O<sub>2</sub>, as shown in Fig. 3). With increasing anneal duration, more recombination active rings appeared around the center. The new rings near the edge of the TR-O<sub>2</sub> samples may be different from the ring defects appearing around the center of the samples. We suspect these rings to be OSFs that delineate the inner vacancy-rich region and the outer self-interstitial rich region.<sup>35</sup>

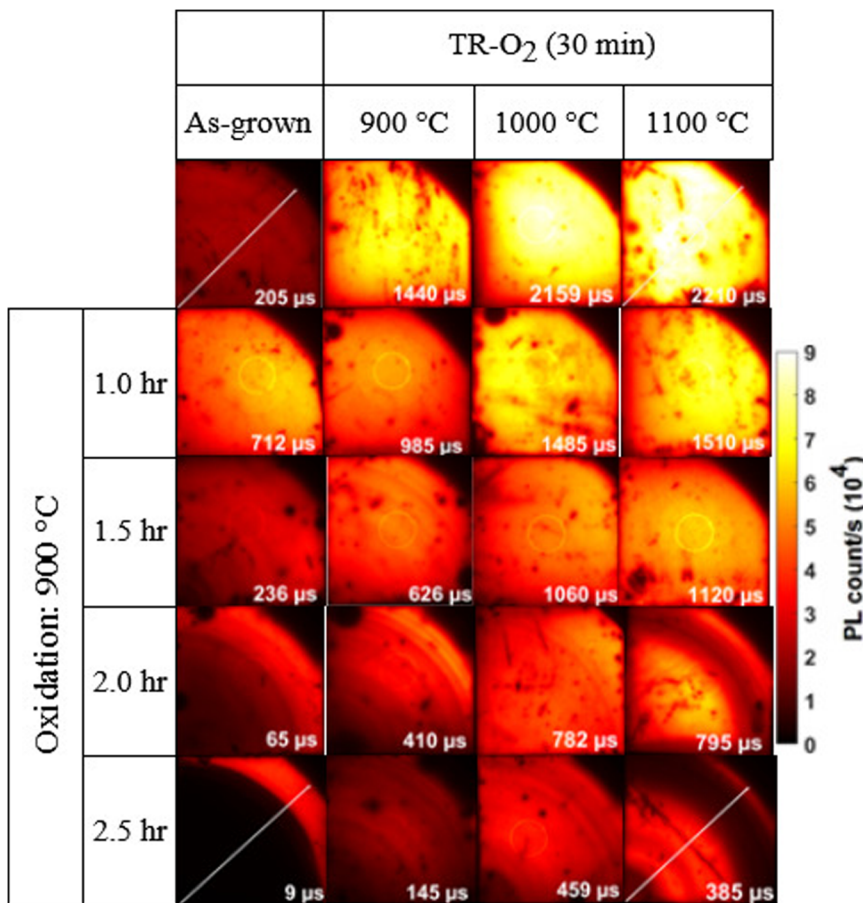


**FIG. 3.** PL images of the as-grown and TR-O<sub>2</sub> (30 min) UMG-Cz samples ( $3 \times 3$  in.<sup>2</sup>) after subsequent oxidation at 900 °C. All of the images were captured at a constant illumination intensity of 0.5 suns and an exposure time of 0.1 s. Effective lifetimes were extracted at an injection level of  $\Delta n = 1 \times 10^{15} \text{ cm}^{-3}$ . The bright circle in some of the images is an artifact due to the conductance coil in the PL imaging tool. The white lines represent the FTIR line scan direction.

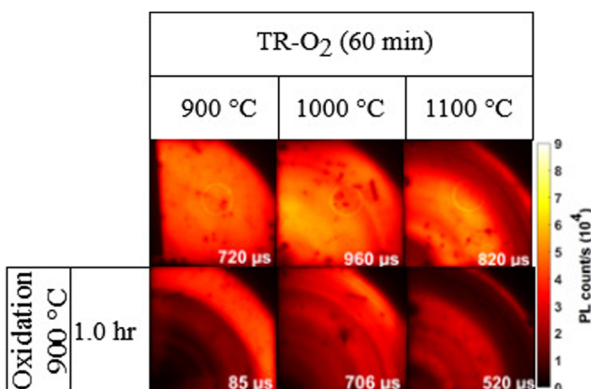


**FIG. 4.** PL images of the as-grown and TR-O<sub>2</sub> (60 min) UMG-Cz samples ( $3 \times 3$  in.<sup>2</sup>) after further oxidation at 900 °C. All of the images were captured at a constant illumination intensity of 0.5 suns and an exposure time of 0.1 s. The effective lifetimes were extracted at an injection level of  $\Delta n = 1 \times 10^{15} \text{ cm}^{-3}$ . The bright circle in some of the images is an artifact due to the conductance coil in the PL imaging tool.

Generally, OSF rings do not exist in the as-grown state, but their nuclei formed during ingot growth.<sup>36</sup> However, with the increase in oxidation temperature, additional self-interstitials are injected into the bulk, straining the OSF nuclei.<sup>37</sup> Then, the strained OSF nuclei tend to grow with the increasing oxidation duration, forming the OSF rings.<sup>38,39</sup> Hence, at the high-temperature oxidation, OSFs tend to be more dominant and appear before ring defects in the center, as exhibited in the 1100 °C TR-O<sub>2</sub> samples in Figs. 3–5.

### C. Ring defects in EG-Cz wafers due to different TR durations

Similar to the UMG-Cz samples, the EG-Cz samples achieved higher effective lifetimes after TR, indicating the bulk lifetime of the electronic-grade wafers used in this work was also partially limited by grown-in OPN. After subsequent oxidation at 900 °C, the as-grown and TR-O<sub>2</sub> EG-Cz samples also showed gradual bulk degradation, eventually forming ring defects, as shown in Figs. 7–9. However, the lifetime degradation in the EG-Cz samples was slower in comparison to the UMG-Cz samples. As a result, the incubation times were longer for the as-grown EG-Cz sample (3 h) in comparison to the as-grown

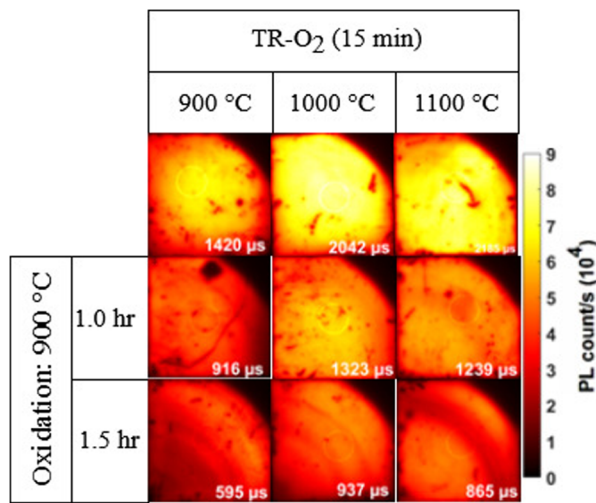


**FIG. 5.** PL images of the as-grown and TR-O<sub>2</sub> (15 min) UMG-Cz samples ( $3 \times 3$  in.<sup>2</sup>) after further oxidation at 900 °C. All of the images were captured at a constant illumination intensity of 0.5 suns and an exposure time of 0.1 s. The effective lifetimes were extracted at an injection level of  $\Delta n = 1 \times 10^{15}$  cm<sup>-3</sup>. The bright circle in some of the images is an artifact due to the conductance coil in the PL imaging tool.

UMG-Cz (1.5 h) sample for the 900 °C oxidation process. This is attributed to the relatively low concentrations of initial [O<sub>i</sub>], [C], and intrinsic point defects in these EG-Cz wafers, as shown in Table I. In general, the incubation time is influenced by several factors such as the thermal budgets, initial [O<sub>i</sub>], [C], ambient, and intrinsic point defects concentrations, all of which affect the re-formation of oxygen precipitates.<sup>32,40</sup>

Furthermore, the EG-Cz samples used in this work showed a similar response to the UMG-Cz samples for the different TR

durations. The degradation was the smallest for the TR-O<sub>2</sub> with 30 min duration, leading to the longest incubation time (6 h), whereas the 60 min TR treatment showed the shortest incubation time (2 h) for ring defects. Thus, these results indicate that the longer TR steps are not necessarily beneficial to improve the bulk quality of Cz wafers.

The striking differences between the UMG-Cz and EG-Cz samples used in this work were the pattern of losses in [O<sub>i</sub>] and the appearance of ring defects during subsequent 900 °C oxidation steps. Unlike the UMG-Cz samples, the global [O<sub>i</sub>] distribution in the EG-Cz samples remained uniform from the center to the edge, as shown in Fig. 6(b), even after subsequent oxidation. Furthermore, the EG-Cz samples used in this work exhibited ring defects distributed quite evenly across the wafer, rather than being concentrated near the center or edge. This suggests that these EG-Cz samples had relatively uniform global intrinsic point defect distributions forming evenly sized grown-in OPN. Note that the as-grown EG-Cz samples did not show any non-uniform appearance of ring defects even after subjecting them to oxidation at 900 °C for 2.25 h, 2.5 h, and 2.75 h long duration (incubation time for the as-grown EG-Cz is 3 h). Nevertheless, ring defects still appeared in these samples after subsequent oxidation steps. This is most likely due to the ingot growth conditions, which affect the radial distribution of intrinsic point defects. Generally, in commercial Cz puller, the growth rate (V) is controlled to be uniform across the radial direction. In this case, a global radial distribution (from center to edge) of intrinsic point defects and impurities should be uniform. However, near the solid/melt interface, the temperature gradient (G) fluctuates due to variations in thermal convection, crystal rotation, and crystal pull rate.<sup>41,42</sup> The temperature variations cause microscopic growth rate fluctuations, which can induce striations of intrinsic point defect concentrations.<sup>43,44</sup> These inhomogeneously incorporated intrinsic point defect concentrations trigger local variations of the oxygen precipitation during the subsequent heat treatments.<sup>45</sup> As a result, we observed fine ring defects in these EG-Cz samples, even though the [O<sub>i</sub>] distribution

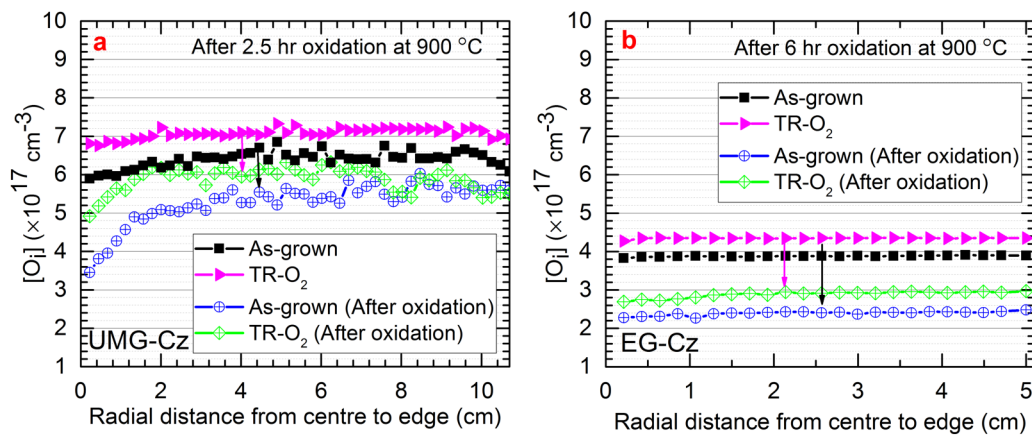


**FIG. 6.** FTIR measured radial distribution of [O<sub>i</sub>] for the as-grown and TR-O<sub>2</sub> (1100 °C for 30 min) samples, (a) for the UMG-Cz samples after 2.5 h of subsequent oxidation at 900 °C and (b) for the EG-Cz samples after 6 h of subsequent oxidation at 900 °C.

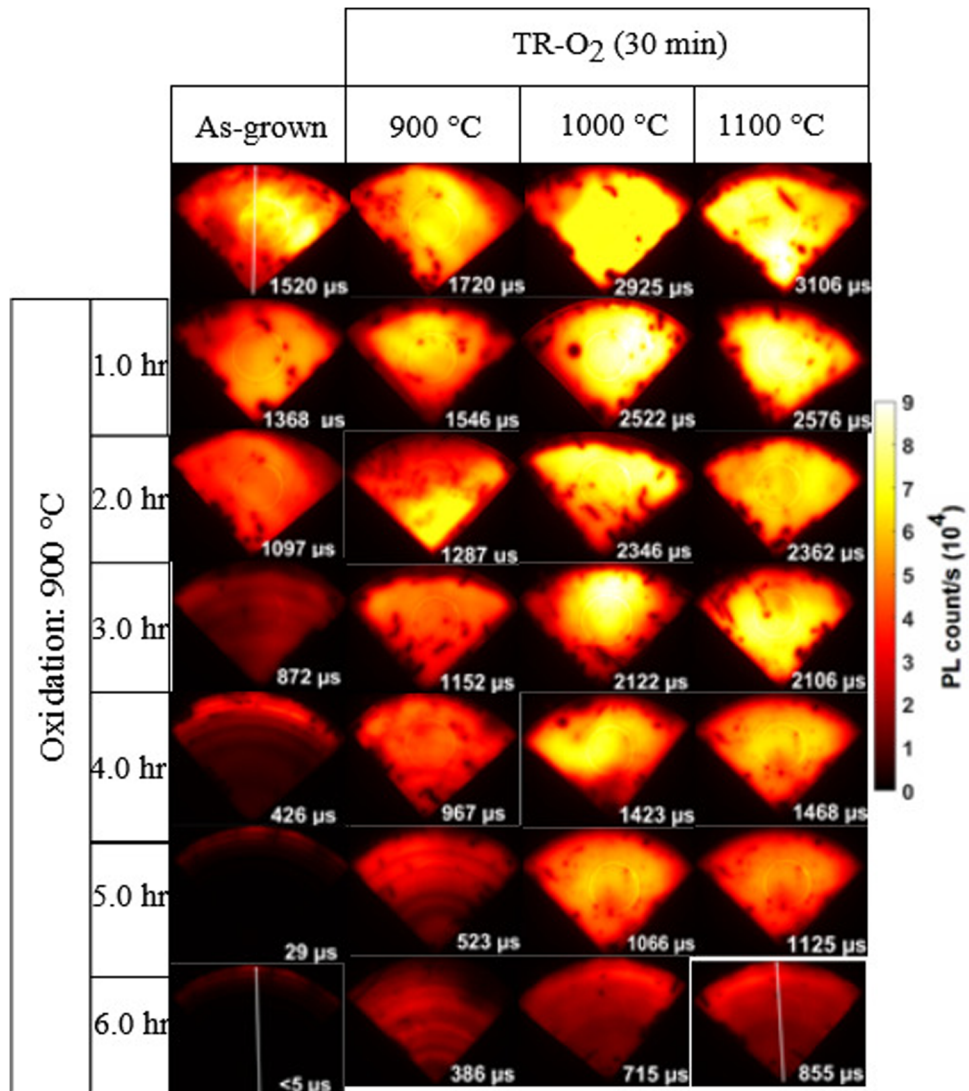


**FIG. 7.** PL images of the as-grown and TR-O<sub>2</sub> (30 min) EG-Cz samples (quarters of 4-in.) after subsequent oxidation at 900 °C. All the images were captured at a constant illumination intensity of 0.5 suns and an exposure time of 0.1 s. The effective lifetimes were extracted at an injection level of  $\Delta n = 1 \times 10^{15} \text{ cm}^{-3}$ . The bright circle in some of the images is an artifact due to the conductance coil in the PL imaging tool. The white lines represent the FTIR line scan direction.

appears to be largely uniform across the wafer, as opposed to being concentrated at the center or edge, as shown in Fig. 6(b).

#### D. Effect of ambient during a TR step

The TR ambient conditions are known to influence the bulk quality due to their role in intrinsic point defect and extended defect generation,<sup>46</sup> which in turn influence the kinetics of oxygen precipitation.<sup>18,47</sup> In this work, we have explored the impact of nitrogen and oxygen ambient during TR at 1100 °C for 30 min. During the 1100 °C TR steps, equal concentrations of vacancies

and interstitials are expected to be generated as Frenkel-pairs in the bulk. Most of these generated vacancy-interstitial pairs recombine in the bulk or diffuse to the surface. However, at 1100 °C, vacancies have a relatively low diffusivity compared to self-interstitials in silicon.<sup>48</sup> Thus, during the TR-O<sub>2</sub> step, the additional injection of self-interstitials from the surface during oxide growth reduces the vacancy concentrations in the bulk,<sup>49</sup> suppressing oxygen precipitation.<sup>18,47</sup> In contrast, in the TR-N<sub>2</sub> samples, no interstitials are injected from the surface, leaving the bulk vacancy-rich,<sup>40,51</sup> and potentially with higher nitrogen concentration, which combines into nitrogen-vacancy and nitrogen-oxygen-vacancy complexes,<sup>51</sup>

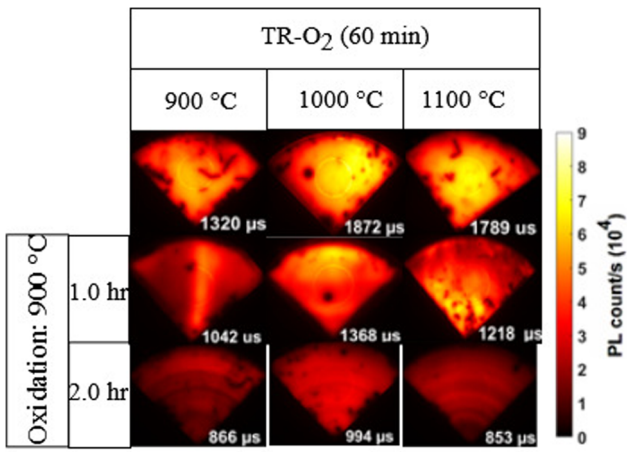


**FIG. 8.** PL images of the as-grown and TR-O<sub>2</sub> (60 min) EG-Cz samples (quarters of 4-in.) after subsequent oxidation at 900 °C. All of the images were captured at a constant illumination intensity of 0.5 suns and an exposure time of 0.1 s. The effective lifetimes were extracted at an injection level of  $\Delta n = 1 \times 10^{15} \text{ cm}^{-3}$ . The bright circle in some of the images is an artifact due to the conductance coil in the PL imaging tool.

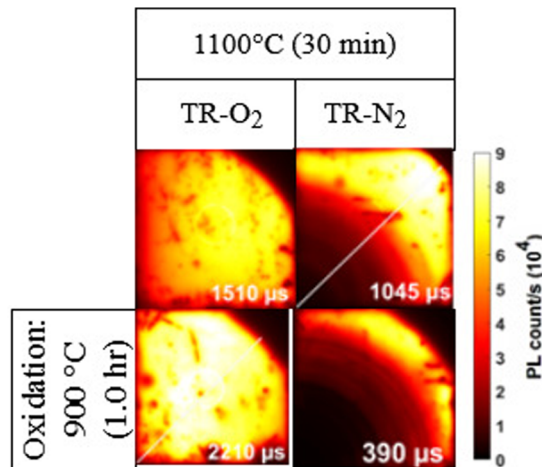


**FIG. 10.** PL images of the TR-O<sub>2</sub> and TR-N<sub>2</sub> (1100 °C) UMG-Cz samples (3 × 3 in.<sup>2</sup>) after subsequent 1 h oxidation at 900 °C. All the images were captured at a constant illumination intensity of 0.5 suns and an exposure time of 0.1 s. The effective lifetimes were extracted at an injection level of  $\Delta n = 1 \times 10^{15} \text{ cm}^{-3}$ . The white lines represent the FTIR line scan direction.

thus enhancing oxygen precipitation. Enhanced precipitation has been corroborated by the appearance of ring defects in the UMG sample, as shown in Fig. 10. Furthermore, the FTIR line scans showed a significantly lower [O<sub>i</sub>] distribution around the center for the TR-N<sub>2</sub>, as shown in Fig. 11. However, [O<sub>i</sub>] distributions toward the edge were similar for both TR-O<sub>2</sub> and TR-N<sub>2</sub> UMG samples.

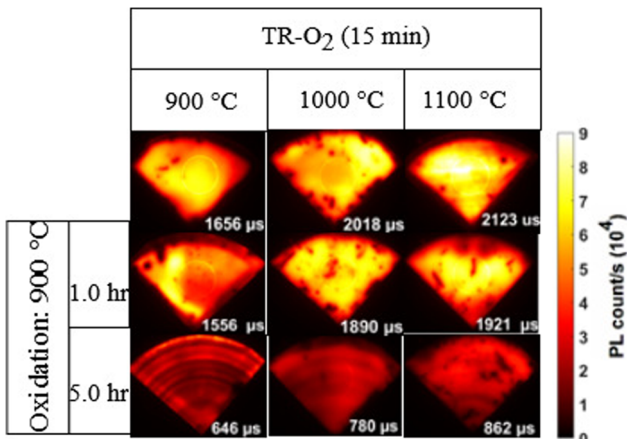


**FIG. 9.** PL images of the as-grown and TR-O<sub>2</sub> (15 min) EG-Cz samples (quarters of 4-in.) after subsequent oxidation at 900 °C. All the images were captured at a constant illumination intensity of 0.5 suns and an exposure time of 0.1 s. The effective lifetimes were extracted at an injection level of  $\Delta n = 1 \times 10^{15} \text{ cm}^{-3}$ . The bright circle in some of the images is an artifact due to the conductance coil in the PL imaging tool.

This could be related to the dominance of the grown-in self-interstitials which retard the oxygen precipitation rate.

The TR-N<sub>2</sub> EG-Cz samples did not show ring defects. However, during subsequent oxidations at 900 °C, the TR-N<sub>2</sub> EG-Cz samples developed ring defects with a shorter incubation time (4 h) in comparison to the TR-O<sub>2</sub> EG-Cz (6 h) samples (PL images not shown here). The two cases showed similar radial [O<sub>i</sub>] distributions, except that the TR-N<sub>2</sub> sample had slightly lower [O<sub>i</sub>] near the center, as shown in Fig. 11.

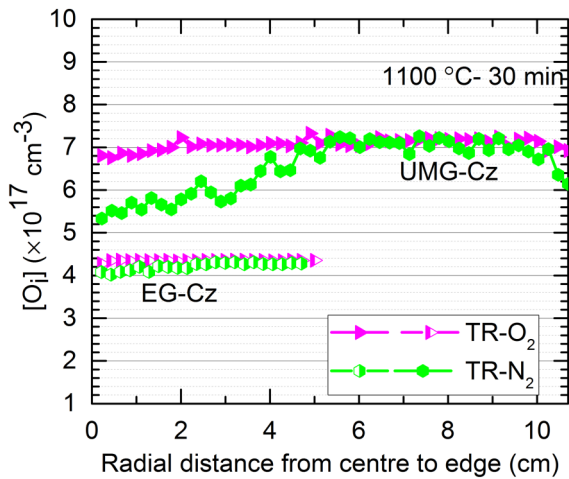


**FIG. 11.** FTIR measured radial distribution of [O<sub>i</sub>] for the UMG-Cz and EG-Cz samples subjected to 1100 °C for 30 min in nitrogen and oxygen ambient.

#### IV. CONCLUSIONS

In summary, we have shown that the TR conditions can strongly influence the formation of ring defects during subsequent thermal treatments of Cz-grown silicon wafers. Both types of Cz wafers used in this work showed a positive response to the TR step. Based on the samples used in this work, the TR temperature range of 1000 °C–1100 °C and the duration of 30 min led to an optimum preservation of the bulk during a subsequent oxidation step at 900 °C. Interestingly, the longer TR durations were not beneficial for mitigating ring defect formation, possibly due to the ripening of undissolved OPN. The UMG-Cz samples were more sensitive to the heat treatments, presumably due to a slightly higher [O<sub>i</sub>] concentration, as well as higher concentrations of other impurities such as C, which can act as the catalyst of oxygen precipitation. As a result, the UMG-Cz samples exhibited shorter incubation times for ring defects than the EG-Cz samples. Furthermore, the UMG-Cz samples lost a higher [O<sub>i</sub>] near the center than toward the edge. As a result, the UMG-Cz samples exhibited a non-uniform appearance of ring defects from either the center or the edge during subsequent heat treatments. However, the EG-Cz samples showed a more uniform distribution of [O<sub>i</sub>] across the wafer, even after subsequent oxidation steps. Unlike in the UMG-Cz samples, the EG-Cz samples developed ring defects that were distributed rather uniformly across the wafer. Finally, the influence of ambient gases on the onset of ring defects in Cz wafers is demonstrated. In this work, both the UMG-Cz and EG-Cz TR-N<sub>2</sub> samples showed shorter incubation times than their TR-O<sub>2</sub> counterparts. Therefore, this work demonstrates that the efficacy of a TR step depends on both the process parameters and the wafer properties.

#### ACKNOWLEDGMENTS

This work has been supported by the Australian Renewable Energy Agency (ARENA) through the Australian Centre for Advanced Photovoltaics (ACAP) and Project No. RND017. Apollon Solar is acknowledged for providing the UMG wafers for this work. R.B. would like to thank Dr. Jordi Veirman and Mickael Albaric for fruitful discussions. Also, Corinne Frigo is thanked for help with the FTIR measurements.

#### DATA AVAILABILITY

The data that support the findings of this paper are available from the corresponding author upon reasonable request.

#### REFERENCES

- <sup>1</sup>V. V. Voronkov and R. Falster, "Grown-in microdefects, residual vacancies and oxygen precipitation bands in Czochralski silicon," *J. Cryst. Growth* **204**(4), 462–474 (1999).
- <sup>2</sup>H. J. Queisser and P. G. G. Van Loon, "Growth of lattice defects in silicon during oxidation," *J. Appl. Phys.* **35**(10), 3066–3067 (1964).
- <sup>3</sup>J. Haunschmid, I. E. Reis, J. Geilker, and S. Rein, "Detecting efficiency-limiting defects in Czochralski-grown silicon wafers in solar cell production using photoluminescence imaging," *Phys. Status Solidi Rapid Res. Lett.* **5**(5–6), 199–201 (2011).
- <sup>4</sup>T. Niewelt *et al.*, "Interstitial oxygen imaging from thermal donor growth—A fast photoluminescence based method," *Sol. Energy Mater. Sol. Cells* **131**, 117–123 (2014).
- <sup>5</sup>L. I. Murin, J. L. Lindström, V. P. Markevich, A. Misiuk, and C. A. Londos, "Thermal double donor annihilation and oxygen precipitation at around 650 °C in Czochralski-grown Si: Local vibrational mode studies," *J. Phys. Condens. Matter* **17**(22), S2237–S2246 (2005).
- <sup>6</sup>W. Götz, G. Pensl, W. Zulehner, R. C. Newman, and S. A. McQuaid, "Thermal donor formation and annihilation at temperatures above 500 °C in Czochralski-grown Si," *J. Appl. Phys.* **84**(7), 3561–3568 (1998).
- <sup>7</sup>J. Osaka, N. Inoue, and K. Wada, "Homogeneous nucleation of oxide precipitates in Czochralski-grown silicon," *Appl. Phys. Lett.* **36**(4), 288–290 (1980).
- <sup>8</sup>M. J. Binns, J. Kearns, and E. A. Good, "(Invited) impact of oxygen-related defects on lifetime degradation in N-type CCZ/CZ mono-crystalline silicon during cell processing," *ECS Trans.* **60**(1), 1233–1238 (2014).
- <sup>9</sup>R. Basnet, C. Sun, H. Wu, H. T. Nguyen, F. E. Rougieux, and D. Macdonald, "Ring defects in n-type Czochralski-grown silicon: A high spatial resolution study using Fourier-transform infrared spectroscopy, micro-photoluminescence, and micro-Raman," *J. Appl. Phys.* **124**(24), 243101 (2018).
- <sup>10</sup>W. Bergholz *et al.*, "A study of oxygen precipitation in silicon using high-resolution transmission electron microscopy, small-angle neutron scattering and infrared absorption," *Philos. Mag. B* **59**(5), 499–522 (1989).
- <sup>11</sup>G. Coletti *et al.*, "Removing the effect of striations in n-type silicon solar cells," *Sol. Energy Mater. Sol. Cells* **130**, 647–651 (2014).
- <sup>12</sup>R. Basnet *et al.*, "Methods to improve bulk lifetime in n-type Czochralski-grown upgraded metallurgical-grade silicon wafers," *IEEE J. Photovoltaics* **8**(4), 990–996 (2018).
- <sup>13</sup>J. D. Murphy, R. E. McGuire, K. Bothe, V. V. Voronkov, and R. J. Falster, "Minority carrier lifetime in silicon photovoltaics: The effect of oxygen precipitation," *Sol. Energy Mater. Sol. Cells* **120**, 402–411 (2014).
- <sup>14</sup>P. Manshanden and P. C. P. Bronsveld, "Investigation of hydrogenation in n-type wafers with ring- and disc-shaped defect zones," *Energy Proc.* **92**, 857–866 (2016).
- <sup>15</sup>B. Hallam, C. Chan, M. Abbott, and S. Wenham, "Hydrogen passivation of defect-rich n-type Czochralski silicon and oxygen precipitates," *Sol. Energy Mater. Sol. Cells* **141**, 125–131 (2015).
- <sup>16</sup>R. Basnet *et al.*, "22.6% efficient solar cells with polysilicon passivating contacts on n-type solar-grade wafers," *Sol. RRL* **3**(11), 1900297 (2019).
- <sup>17</sup>P. C. P. Bronsveld, P. Manshanden, A. Gutjahr, M. Koppes, and I. G. Romijn, "The effect of n-pasha processing on bulk wafer quality," in *Proceedings of the 31st European Photovoltaic Solar Energy Conference (EUPVSEC)*, Hamburg, Germany, 2015.
- <sup>18</sup>V. LaSalvia, *et al.*, "Tabula rasa for n-Cz silicon-based photovoltaics," *Prog. Photovoltaics Res. Appl.* **27**(2), 136–143 (2019).
- <sup>19</sup>B. Sopori, *et al.*, "Dissolution of oxygen precipitate nuclei in n-type CZ-Si wafers to improve their material quality: Experimental results," *IEEE J. Photovoltaics* **7**(1), 97–103 (2017).
- <sup>20</sup>G. Kissinger, *et al.*, "Analytical modeling of the interaction of vacancies and oxygen for oxide precipitation in RTA treated silicon wafers," *J. Electrochem. Soc.* **154**(6), H454 (2007).
- <sup>21</sup>R. Falster, V. V. Voronkov, and F. Quast, "On the properties of the intrinsic point defects in silicon: A perspective from crystal growth and wafer processing," *Phys. Status Solidi B* **222**(1), 219–244 (2000).
- <sup>22</sup>R. Einhaus, J. Kraiem, S. Martinuzzi, and M. C. Record, "PHOTOSIL—Simplified production of solar silicon from metallurgical silicon," in *Proceedings of the 21st European Photovoltaic Solar Energy Conference (EUPVSEC)*, Dresden, Germany, 2006, pp. 580–584.
- <sup>23</sup>B. L. Sopori, Y. Zhang, and R. Reedy, "H diffusion for impurity and defect passivation: A physical model for solar cell processing," in *Conference Record of the Twenty-Ninth IEEE Photovoltaic Specialists Conference, 2002* (IEEE, Orleans, 2002), pp. 222–226.
- <sup>24</sup>C. Leguijt, *et al.*, "Low temperature surface passivation for silicon solar cells," *Sol. Energy Mater. Sol. Cells* **40**(4), 297–345 (1996).
- <sup>25</sup>R. A. Sinton and A. Cuevas, "Contactless determination of current-voltage characteristics and minority-carrier lifetimes in semiconductors from quasi-steady-state photoconductance data," *Appl. Phys. Lett.* **69**(17), 2510–2512 (1996).

- <sup>26</sup>F. Schindler, *et al.*, “Modeling majority carrier mobility in compensated crystalline silicon for solar cells,” *Sol. Energy Mater. Sol. Cells* **106**, 31–36 (2012).
- <sup>27</sup>T. Trupke, R. A. Bardos, M. C. Schubert, and W. Warta, “Photoluminescence imaging of silicon wafers,” *Appl. Phys. Lett.* **89**(4), 044107–044107 (2006).
- <sup>28</sup>R. C. Newman, “Oxygen diffusion and precipitation in Czochralski silicon,” *J. Phys. Condens. Matter* **12**(25), R335–R365 (2000).
- <sup>29</sup>R. J. Falster, M. Cornara, D. Gambaro, M. Olmo, and M. Pagani, “Effect of high temperature pre-anneal on oxygen precipitates nucleation kinetics in Si,” *Solid State Phenom.* **57–58**, 123–128 (1997).
- <sup>30</sup>P. Wang, C. Cui, X. Yu, and D. Yang, “Growth and ripening of oxygen precipitation in neutron-irradiated Czochralski silicon,” *Mater. Sci. Semicond. Process.* **74**, 369–374 (2018).
- <sup>31</sup>F. Shimura, “Carbon enhancement effect on oxygen precipitation in Czochralski silicon,” *J. Appl. Phys.* **59**(9), 3251–3254 (1986).
- <sup>32</sup>S. Zhang, M. Juel, E. J. Øvrelid, and G. Tranell, “Investigating the effect of carbon on oxygen behavior in n-type Czochralski silicon for PV application,” *J. Cryst. Growth* **411**, 63–70 (2015).
- <sup>33</sup>J. D. Murphy, K. Bothe, V. V. Voronkov, and R. J. Falster, “On the mechanism of recombination at oxide precipitates in silicon,” *Appl. Phys. Lett.* **102**(4), 042105 (2013).
- <sup>34</sup>H. Zimmermann and H. Ryssel, “An investigation of vacancy concentrations in bulk silicon,” *MRS Proc.* **262**, 31 (1992).
- <sup>35</sup>V. V. Voronkov, “The mechanism of swirl defects formation in silicon,” *J. Cryst. Growth* **59**(3), 625–643 (1982).
- <sup>36</sup>K. Marsden, T. Kanda, M. Okui, M. Hourai, and T. Shigematsu, “Determination of the criteria for nucleation of ring-OSF from small as-grown oxygen precipitates in CZSi crystals,” *Mater. Sci. Eng.: B* **36**(1–3), 16–21 (1996).
- <sup>37</sup>M. E. Law, Y. M. Haddara, and K. S. Jones, “Effect of the silicon/oxide interface on interstitials: Di-interstitial recombination,” *J. Appl. Phys.* **84**(7), 3555–3560 (1998).
- <sup>38</sup>M. Hasebe, Y. Takeoka, S. Shinoyama, and S. Naito, “Formation process of stacking faults with ringlike distribution in CZ-Si wafers,” *Jpn. J. Appl. Phys.* **28**(Part 2, No. 11), L1999–L2002 (1989).
- <sup>39</sup>R. A. Brown, Z. Wang, and T. Mori, “Engineering analysis of microdefect formation during silicon crystal growth,” *J. Cryst. Growth* **225**(2–4), 97–109 (2001).
- <sup>40</sup>R. Falster and V. Voronkov, “The engineering of intrinsic point defects in silicon wafers and crystals,” *Mater. Sci. Eng. B* **73**(1–3), 87–94 (2000).
- <sup>41</sup>K. S. Choe, “Growth striations and impurity concentrations in HMCZ silicon crystals,” *J. Cryst. Growth* **262**(1–4), 35–39 (2004).
- <sup>42</sup>A. J. R. De Kock, P. J. Roksnor, and P. G. T. Boonen, “Formation and elimination of growth striations in dislocation-free silicon crystals,” *J. Cryst. Growth* **28**(1), 125–137 (1975).
- <sup>43</sup>T. Abe, “The growth of Si single crystals from the melt and impurity incorporation mechanisms,” *J. Cryst. Growth* **24–25**, 463–467 (1974).
- <sup>44</sup>J. A. Burton, R. C. Prim, and W. P. Slichter, “The distribution of solute in crystals grown from the melt. Part I. Theoretical,” *J. Chem. Phys.* **21**(11), 1987–1991 (1953).
- <sup>45</sup>A. J. R. de Kock, “Vacancy clusters in dislocation-free silicon,” *Appl. Phys. Lett.* **16**(3), 100–102 (1970).
- <sup>46</sup>C. Cui, D. Yang, X. Ma, R. Fan, and D. Que, “Effect of annealing atmosphere on oxygen precipitation and formation of denuded zone in Czochralski silicon wafer,” *Phys. Status Solidi Appl. Mater. Sci.* **203**(10), 2370–2375 (2006).
- <sup>47</sup>F. E. Rougieux, H. T. Nguyen, D. H. Macdonald, B. Mitchell, and R. Falster, “Growth of oxygen precipitates and dislocations in Czochralski silicon,” *IEEE J. Photovoltaics* **7**(3), 735–740 (2017).
- <sup>48</sup>V. V. Voronkov and R. Falster, “The diffusivity of the vacancy in silicon: Is it fast or slow?” *Mater. Sci. Semicond. Process.* **15**(6), 697–702 (2012).
- <sup>49</sup>N. Jeng and S. T. Dunham, “Interstitial supersaturation during oxidation of silicon in steam ambients,” *J. Appl. Phys.* **72**(5), 2049–2053 (1992).
- <sup>50</sup>V. V. Voronkov, R. Falster, T. Kim, S. Park, and T. Torack, “Depth profiles of oxygen precipitates in nitride-coated silicon wafers subjected to rapid thermal annealing,” *J. Appl. Phys.* **114**(4), 043520 (2013).
- <sup>51</sup>X. Yu, D. Yang, X. Ma, J. Yang, L. Li, and D. Que, “Grown-in defects in nitrogen-doped Czochralski silicon,” *J. Appl. Phys.* **92**(1), 188–194 (2002).